School of Chemistry

MPhil Thesis

Exploring Cation Diffusion to Redox Species Encapsulated in Carbon Nanotubes

Beth Mortiboy

14250465

Supervisors: Dr Darren Walsh and Dr Graham Newton

27 August 2021

ABSTRACT

The transport of ions through carbon nanotube systems has been studied extensively. However, there is limited evidence of ion transport via nanotube sidewalls. Using a novel host-guest redox active hybrid material, insight into the mechanisms of ion transport within carbon nanotubes can be assessed using very simple electrochemical techniques. Here we utilise a system whereby polyoxometalates (POMs) are encapsulated within single-walled carbon nanotubes (SWNTs). The POM acts as a redox probe and can measure the effectiveness of ion transport throughout the material. The diffusion of large cationic species (Li^+, Na^+, K^+, NH_4^+) throughout the system is limited and the mechanism of their transport can be confirmed using a simple blocking technique, whereby the open ends of the SWNT become inaccessible to such ions. The kinetic isotope effect of proton and deuteron transport throughout the systems was found to be 1.32 and 1.21 for two aqueous acidic electrolyte systems. This value is significantly lower than what is reported for other systems focusing on the permeation of these ions through similar one-atom thick membranes. It can be concluded that for practical application within electrochemical systems, the rate of transport of both H^+ and D^+ is sufficiently fast and that the permeation of these ions through the nanotube system is not rate limiting.

Contents

1. Introduction

The transport of ions across nanoscale membranes has been widely studied for a variety of carbon-based systems.[1–4] Including the interlayer spacing between two-dimensional (2D) graphene monolayers, carbon nanotube (CNT) nanochannels and most notably, hydron (H^+/D^+) transport through atomically thin barriers i.e. monolayers of graphene. A fundamental understanding of the mechanisms of ion transport is imperative, to effectively utilize a system that relies on ion transport for applications such as separation, sensing and energy storage technologies.[5-15] Studies have been completed assessing the mechanisms of ion transport through one atom thick membranes, most notably by Mogg et al. whereby a graphene monolayer was isolated and used within ion-selectivity measurements. The results of such experiments were astonishing and provided evidence for the perfect selectivity of protons through crystals that can be considered free of atomic-scale defects. The process of collecting these results required the fabrication of a device able to isolate a single graphene layer. The layer is typically isolated using micromechanical cleavage, however, this process can be imprecise and time consuming.[16] Once isolated the crystal is clamped into a device suitable to separate two solutions, requiring specialised equipment. Here we utilize a very simple system to understand mechanisms of ion transport and provide insight into the selective nature of carbon nanotube-based materials.

The formation of novel host-guest redox active hybrid materials has recently been reported.[17] Within this report the spontaneous encapsulation of polyoxometalates (POMs) within single walled carbon nanotubes (SWNTs) is outlined using an outstandingly simple method, requiring no specialised equipment.

1.1 Polyoxometalates

POMs are large anionic metal oxygen clusters of early transition metal elements and have exceptional properties, both physical and chemical, due to their structural diversity.[18] They contain multiple metal centres connected within an oxide framework.

The two basic structures of POMs are Keggin and Dawson. Keggin POMs consist of 12 metal atoms arranged around a single heteroatom and take the general form of $[XM_{12}O_{40}]$. With the Dawson (also known as Wells-Dawson) POM being a dimer, formed from the combination of two lacunary Keggin monomers $[XW_9O_{34}]^{z-}$, the resulting structures consist of 18 metal atoms arranged around 2 heteroatoms and take the general form of $[X_2M_{18}O_{62}]$.[18,19]

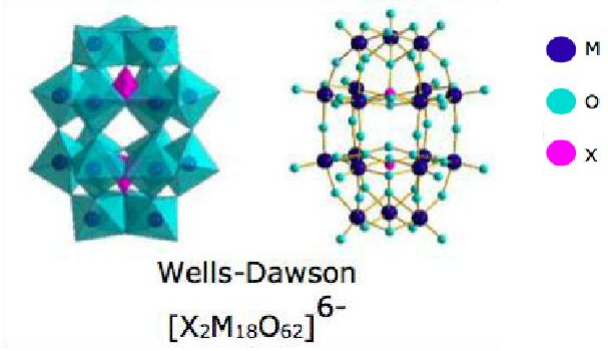

Figure 1. *Polyhedron and ball and sticks models of the typical POM structures of Wells-Dawson heteropolyoxoanions. The metal atoms are shown at the centre of the polyhedra, with an oxygen atom at every vertex. X represents template anions, which are seen at the centre of the structure.*[20]

Previous research showed that the redox behaviour exhibited by hybrid materials containing the tungsten Wells-Dawson anions, $[P_2W_{18}O_{62}]^{6-}$,$\{W_{18}\}$, as the POM species was well-defined and stable.[21] As a result, this research utilises the $\{W_{18}\}$ POM as the redox active species within the novel host-guest hybrid materials.

1.2 POM@SWNT Hybrid Material

POMs in isolation exhibit promising properties for electrochemical energy storage applications[22] as they can undergo fast reversible multi-electron transfer reactions.[19] However, the success of POMs alone for such applications is impeded. When fully oxidized, POMs are electrically insulating, meaning charge flow between the redox centres and the electrode is limited. By dispersing the POM in a highly conductive substrate such as carbon nanotubes the maximum concentration of POM becomes electrochemically accessible.[23,24] The novel immobilization of POMs within CNTs not only provides a conductive support for the POM, but also acts as a protective barrier against instabilities caused by the external environment.

1.2.1 Synthesis and Characterisation

The synthesis of POMs encapsulated within SWNT is a simple process, starting with the oxidation of SWNTs. SWNTs have closed tips which need to be removed to allow access to the interior of the nanotube. Heating to 600℃ for 30 minutes opens the tips of the nanotubes, as this surpasses the oxidation temperature of the SWNTs. At this temperature, only the tips are oxidised due to the more reactive nature of the sp^2 hybridised carbon atoms found in the tips. Once opened, the SWNTs were added to an aqueous solution of POM, sonicated, and then stirred for two days at room temperature.[21]

Electron density is transferred from the SWNTs to the POMs when the two species are combined in solution and sonicated, this creates a coulombic attraction, resulting in the electrostatically driven encapsulation of POMs within SWNTs. By carefully selecting specific POM and SWNT species the interior surface interaction can be maximised, aiding the encapsulation. The tungsten Wells-Dawson anions,

$[P_2W_{18}O_{62}]^{6-}$,{W_{18}}, have complementary crystallographic dimensions (approx.1.2 x 1 nm)[25] with the SWNT used (approx. 1.4 nm)[26]. Resulting in densely filled {W_{18}}@SWNT hybrids.

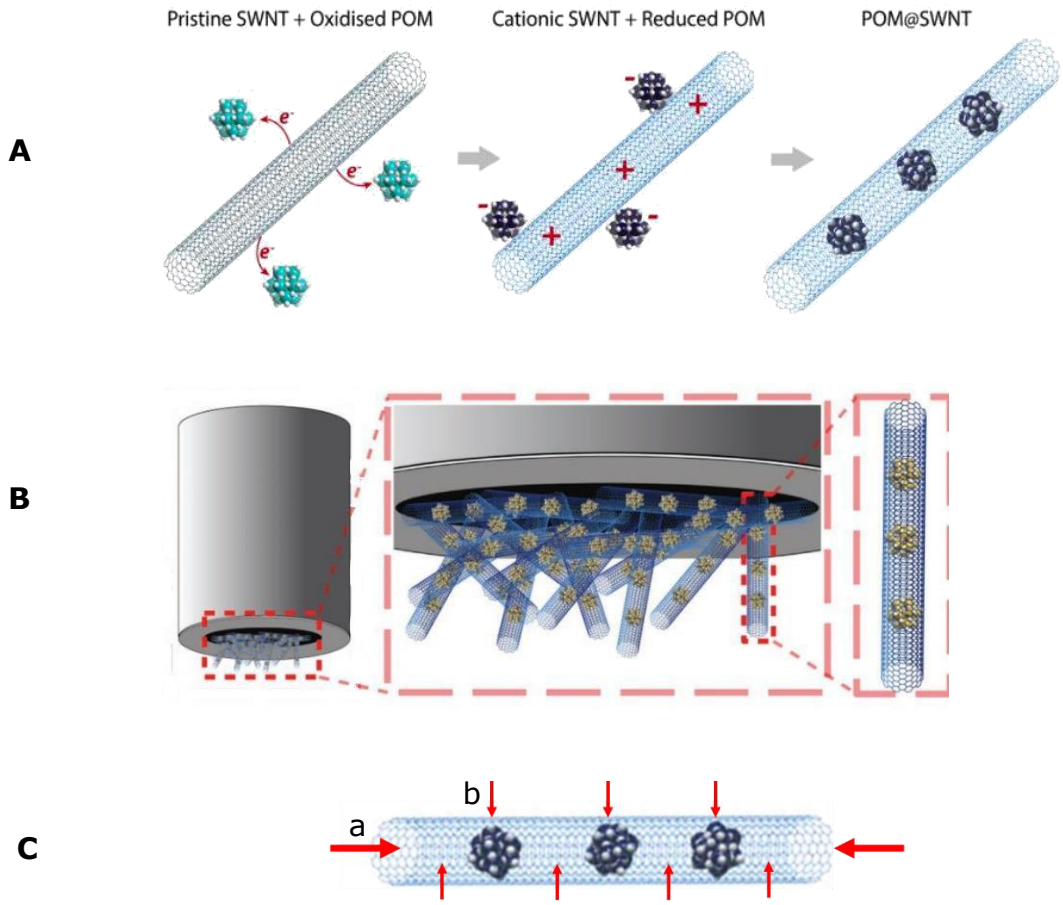

Figure 2. *(A) Schematic showing the redox mechanism resulting in the encapsulation of POMs within SWNTs. (B) Schematic of POM@SWNT adsorbed onto the electrode surface. (C) Schematic demonstrating the potential routes of ion transport to the encapsulated POM.*

On encapsulation of the POMs within the SWNTs, the aqueous solution of POM turns blue (from a clear colourless solution) indicating a charge transfer reaction has occurred as the blue colour is characteristic of reduced POMs.[27,28]

Transmission electron microscopy (TEM) and energy dispersive x-ray (EDX) analysis was used to confirm the encapsulation of POMs within the SWNTs, by providing visual and qualitative evidence (Figure A1).[21]

1.2.2 Ion Transport

These hybrids provide us with an ideal tool to study ion transport throughout carbon nanotube systems. POMs typically exhibit kinetically fast electrochemistry which can be considered not limited by either electron or ion transport.[19] On encapsulation, this electrochemistry is preserved (Figure 3A), however, it is dependent on the electrolyte environment. For electron transfer to successfully occur at the POM there is a requirement for the diffusion of ions throughout the electrolyte solution, this ensures the electrical neutrality of the system is maintained.[29] It is therefore rational to conclude that by studying the electrochemistry of the encapsulated redox active species that behaviour of the ions within solution (namely the cationic species) can be evaluated. Here we use the simple electrochemical method of analysis, cyclic voltammetry, as a tool to provide invaluable insight into the mechanisms of ion diffusion throughout the system.

Cyclic voltammetry is an electrochemical method which measures the change in current as voltage sweeps between set potential limits. The fluctuations in current correspond to reduction and oxidation processes of the species being analysed.[29]

The electrochemistry of a $\{W_{18}\}$@SWNT film immobilized on a glassy-carbon electrode (Figure 2B) in a selection of aqueous supporting electrolytes is studied. By varying both the cationic and anionic species within the electrolyte allows us to discover individually their influence on the POM electrochemistry, which can be directly related to the diffusion of the ions towards the POM via the nanotube barrier. The electrolytes studied are as follows (all electrolytes used were at a concentration of 1.0 $moldm^{-3}$): HCl, H_2SO_4, $HClO_4$, DCl, D_2SO_4, $DClO_4$, LiCl, $LiClO_4$, NaCl, Na_2SO_4, KCl, NH_4Cl.

To enable successful electron transfer to occur, oppositely charged cationic species are required to interact with the encapsulated POM to counterbalance any charge generated during the redox events. The cations within the electrolyte can get sufficiently close the encapsulated POM via one of two routes (Figure 2C): (a) the ions enter the SWNT via the open ends and flow through the interior SWNT channel to access the POM, (b) the ions diffuse through the SWNT sidewalls. A variety of both acidic and non-acidic electrolytes are used within this study to gain insight into the mechanisms of ion transport for a selection of cationic species of varying ionic radii: H^+, D^+, Li^+, Na^+, K^+, NH_4^+.[30]

Entering the SWNT via the open ends is the most likely path for all the cationic species discussed within this study, as the barrier to do so will be the smallest for this route.[2,31] Sterically there is little resistance to any of the hydrated cations from entering the CNT. However, the POMs deeper within the densely filled nanotube cavity will only be accessible to H^+ and D^+ as there is complete steric exclusion of the larger cations, which are unable to permeate through the ~0.2nm gap between the POM and the interior SWNT sidewall.[3] Ultra-fast hydron transport rates are to be expected in these hydrophobic nanochannels.[32] The level of confinement displayed by these narrow cavities facilitated the formation of one-dimensional water chains that enable the transport of H^+ and D^+ towards the interior encapsulated POMs via the Grotthuss mechanism.[32]

The understanding of proton and deuteron abilities to permeate through one-atom-thick crystals such as the SWNT sidewalls is an area of much interest. Although the study of a SWNT system seems to be neglected, the hexagonal lattice of SWNT sidewall is almost directly comparable to that of graphene which has been studied.[33,34] Under ambient conditions a pristine, defect-free graphene monolayer is widely regarded as impermeable to all atoms.[1,2,35] Accelerated

protons and to a lesser extent deuterons are able to penetrate the dense electron cloud surrounding the hexagonal lattice of a graphene monolayer when subjected to a potential bias or at elevated temperatures.[1,2,35,36]

1.3 Aims

The new and novel nature of POM@SWNT hybrid materials results in the need for general improvements in the understanding of the electrochemistry of these materials. The main objectives of this research is to:

- investigate cation transport through the carbon nanotube system, using the electrochemistry of the encapsulated POM to achieve this
- use data collected to support understanding for a proposed mechanism of ion transport throughout the carbon nanotube system
- investigate the kinetic isotope effect of proton and deuteron transport throughout the POM@SWNT system

2. {W_{18}}@SWNT Electrochemistry

Typical surface-confined voltammetry is displayed by the {W_{18}}@SWNT film (Figure 3), as both the oxidized and reduced form of the redox species are strongly absorbed to the electrode. In ideal conditions, {W_{18}}@SWNT displays three clearly defined two-electron redox couples, which can be attributed to the following redox processes[37,38]:

$$P_2W_{18}O_{62}{}^{6-} + 2e^- \leftrightarrow P_2W_{18}O_{62}{}^{8-} \quad (1)$$

$$P_2W_{18}O_{62}{}^{8-} + 2e^- + 2H^+ \leftrightarrow H_2P_2W_{18}O_{62}{}^{8-} \quad (2)$$

$$H_2P_2W_{18}O_{62}{}^{8-} + 2e^- + 2H^+ \leftrightarrow H_4P_2W_{18}O_{62}{}^{8-} \quad (3)$$

The three redox couples will be referred to as {P_2W_{18}}$^{8-}$, {$H_2P_2W_{18}$}$^{8-}$ and {$H_4P_2W_{18}$}$^{8-}$ henceforth, referencing the reduction product of each redox couple. As the {$H_2P_2W_{18}$}$^{8-}$ and {$H_4P_2W_{18}$}$^{8-}$ redox events are proton coupled/cation dependent it is thought that the peak potentials corresponding to these processes may be particularly sensitive to the electrolyte environment.[39] This ideal surface-confined redox behaviour is not displayed for all electrolyte environments studied here, indicating the importance and influence the supporting electrolyte can have on the system.

The impact of encapsulation can be seen by comparing the electrochemistry of the surface confined {W_{18}} film in acidic electrolyte (Figure 3B). Similar potentials are measured when in acidic electrolytes, suggesting that the presence of the carbon nanotube matrix does not limit the transport of protons to the POM. If the SWNT presented a large barrier to the protons, a negative shift in potential would be expected. The voltammograms for {W_{18}} in isolation generally display larger ΔE_P values, which can be attributed to the lack of conductive substrate (SWNT) which usually facilitates the electron transport between the electrode surface and the POM, hence slower redox processes can be expected.[23,24]

The solution phase electrochemistry of $\{W_{18}\}$ in isolation results in four redox couples; two one-electron processes, followed by two two-electron processes (Figure 3A). Typically, only in strong acidic environments i.e. 12.4 mol dm^{-3} will the $\{W_{18}\}$ undergo three two-electron reversible redox processes as seen in the immobilized enivronment.[37] This indicates that the energetics of electron transfer change as a result of confinement and is less affected by pH than when in solution. However, as with the solution phase electrochemistry negative shifts in the peak potentials are still seen with increasing pH for the immobilized equivalents (Figure 3E).

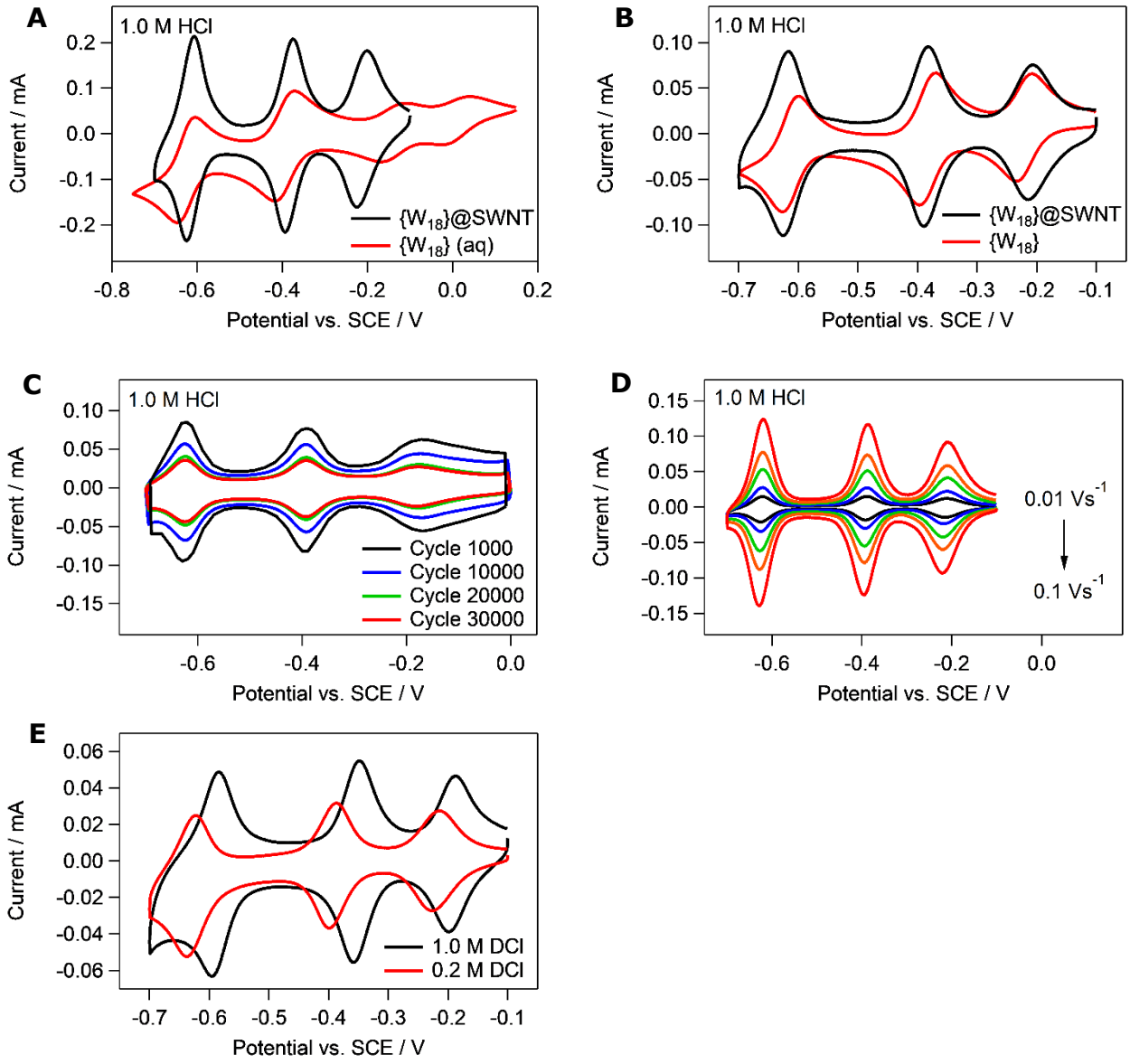

Figure 3. *(A) Cyclic voltammogram of immobilized {W_{18}}@SWNT (black) and solution phase {W_{18}} (red), both recorded at 0.1 V s^{-1} in 1.0 mol dm^{-3} HCl. (B) Cyclic voltammogram of immobilized {W_{18}}@SWNT (black) and immobilized {W_{18}} (red), both recorded at 0.1 V s^{-1} in 1.0 mol dm^{-3} HCl. (C) 1,000th to 30,000th cyclic voltammograms of {W_{18}}@SWNT deposited onto a glassy carbon electrode and cycled at 0.1 V s^{-1} in 1.0 mol dm^{-3} HCl. (D) Cyclic voltammograms of {W_{18}}@SWNT at increasing scan rates; 0.01 V s^{-1} (black), 0.02 V s^{-1} (blue), 0.04 V s^{-1} (green), 0.06 V s^{-1} (orange), 0.1 V s^{-1} (red) in 1.0 mol dm^{-3} HCl. A plot of peak-to-peak separation as a function of scan rate for the three redox couples can be found in the appendix (Figure A2). (E) Cyclic voltammogram of immobilized {W_{18}}@SWNT recorded at 0.1 V s^{-1} in 1.0 mol dm^{-3} DCl (black) and 0.2 mol dm^{-3} DCl (red). A negative shift in peak potential is observed with increasing pH (1.0 mol dm^{-3} → 0.2 mol dm^{-3}).*

2.1 $\{W_{18}\}$@SWNT Electrochemistry in Non-Acidic Electrolytes

When the material is studied in non-acidic electrolytes inconsistent and unstable voltammograms are recorded. By the 50th potential sweep there is little to no electrochemical activity remains for all systems studied (Figure 4A). Example cyclic voltammograms of $\{W_{18}\}$@SWNT in non-acidic electrolytes can be found in the appendix (Figure A3).

Characteristically, a large current is passed during the first reduction process ($\{P_2W_{18}\}^{6-} \rightarrow \{P_2W_{18}\}^{8-}$), currents of such magnitude are not reached for any of the subsequent reduction processes or their corresponding oxidations. This feature suggests initially there is a larger flow of the cationic species from the electrolyte towards the encapsulated redox species. As the charge generated is unmatched for the $\{H_2P_2W_{18}\}^{8-}$ and $\{H_4P_2W_{18}\}^{8-}$ redox events, this indicates that the initial flow of cations towards the POM during the first reduction blocks further diffusion of the cationic species throughout the carbon matrix.

Variation is seen in the potential onset position associated to the first reduction event, which shifts depending on the electrolyte the cyclic voltammogram is recorded in. At 0.1 Vs^{-1} the potential vs. SCE for the first reduction for each environment is as follows: 1.0 mol dm^{-3} $LiClO_4$ (-0.221 V), 1.0 mol dm^{-3} LiCl (-0.286 V), 1.0 mol dm^{-3} NaCl (-0.367 V), 1.0 mol dm^{-3} Na_2SO_4 (-0.368 V), 1.0 mol dm^{-3} NH_4Cl (-0.393 V), 1.0 mol dm^{-3} KCl (-0.415 V). As the ionic radii of the cation in the supporting electrolyte increases, more negative potentials are required for the reduction reaction to occur. Suggesting there is a higher barrier to electron transfer when in environments involving larger cationic species. The extent of pore blocking is seen to reflect changes in hydration shell $K^+ > Na^+ > NH_4^+ > Li^+$[10]. Ionic radii are inversely related to the hydrated cation radii[40], with Li^+ having the largest hydration shell, suggesting that for these electrolytes the diffusion of the ions

through solution and the loss of their hydration shell are not rate limiting steps. It is the ease at which the cation can interact with the POM that appears to be the major influence on the electrochemical behaviour of the {W_{18}}@SWNT system. Results such as these are not unexpected. The nanochannel formed between the nanotube interior and the POM results in steric rejection of the ions with the larger hydrated radii.[3] For the non-acidic electrolytes studied here the estimated hydrated radii of the cation species range from 1.75 to 2.50 Å.[30] It is also due to steric factors that the route of ion transport to the POM can be confirmed as only via the open ends of the nanotube.[1,2] Once these passages to the POMs start to be blocked[41] the number of accessible POMs reduce, therefore resulting in the smaller currents measured on consequent potential sweeps. This blocking process will continue until there are no accessible POMs to these larger cations and the {W_{18}}@SWNT composite becomes essentially electrochemically inactive. Some activity can be regained by cycling in acidic electrolytes once this has occurred, indicating that although the POM is inaccessible to larger cations, protons can still engage with the encapsulated POMs due to their smaller ionic radii (Figure 4B).

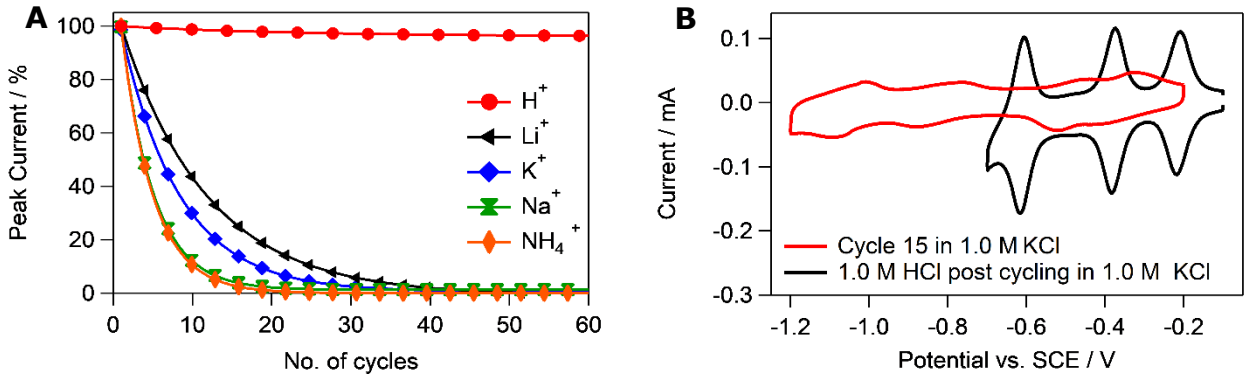

Figure 4. *(A) Average changes in peak currents for {W_{18}}@SWNT in supporting electrolytes containing different cationic species: H^+ (red), Li^+ (black), K^+ (blue), Na^+ (green) and NH_4^+(orange). (B) Cyclic voltammogram of the fifteenth cycle of immobilized {W_{18}}@SWNT recorded at 0.1 V s^{-1} in 1.0 mol dm^{-3} KCl (red). Overlaid with a cyclic voltammogram of the same system cycled in 1.0 mol dm^{-3} HCl post cycling fifteen times in 1.0 mol dm^{-3} KCl (black).*

2.2 {W_{18}}@SWNT Electrochemistry in Acidic Electrolytes

Unlike when in non-acidic electrolytes the electrochemistry in acidic environments is extraordinary. Three clearly defined redox processes are observed whereby rapid electron transfer occurs between the electrode surface and the immobilized {W_{18}}@SWNT. This is evident with only marginal increases in ΔE_P observed with increasing scan rate (Figure 3D). Minor changes in peak-to-peak separations are observed (approx. 25 mV increase as scan rate increases from 0.01 to 1 Vs^{-1}) until the voltammograms are recorded at much higher scan rates.

The {W_{18}}@SWNT system remains electrochemically active after over 30,000 cycles (Figure 3C). This stability is expected to continue over prolonged cycling as the rate at which the current decreases, itself decreases over prolonged cycling. An initial decrease of approximately 51% is seen between the peak current of the first and one thousandth cycle (Figure A4). To see a similar decrease in peak current, the system must be subjected to almost another thirty thousand potential cycles. At which point, the {W_{18}}@SWNT film continues to be electrochemically active, with all three redox processes remaining clearly accessible.

This stability is hugely contrasting to that seen in non-acidic electrolyte systems (Figure 4A), clearly demonstrating the influence the cationic species can have on the capabilities of this redox-active hybrid material. All of this indicates that the proton is the optimal cationic species to allow efficient redox chemistry to occur.

It is important to note that this prolonged stability cannot be recorded in a system where a Pt counter electrode is used. Often in POM voltammetry, features are seen which are commonly attributed to the formation of POM-derived hydrogen evolution; typically, a large increase in cathodic current seen at negative potentials. Recently, it has been proven that this characteristic can instead be a

direct result of dissolve Pt in the solution migrating onto the working electrode surface, catalysing the hydrogen evolution reaction.[42] As a result, a glassy carbon counter electrode has been used throughout the experiments detailed within this study.

2.3 'Capped' {W_{18}}@SWNT Electrochemistry

As ion transport within acidic electrolytes does not appear to be limited by the presence of the SWNT matrix, indicating that protons can readily flow to the encapsulated POMs with little restriction. This transport could be via both mechanisms previously discussed. In hope to isolate the ion diffusion via the nanotube sidewalls, the open ends of the nanotubes were 'capped' to block the flow of ions via this route. A simple method of capping was utilized. By applying 2.77 mM fullerene (C_{60}) in toluene suspension to the {W_{18}}@SWNT film, the ends of the SWNTs become blocked by a large carbon matrix (Figure 5A).

When a vacant SWNT system is subjected to this treatment, the interior of the nanotube becomes densely filled with C_{60} (Figure 5B). As the nanotubes within the {W_{18}}@SWNT system are already filled, the addition of C_{60} does not result in the carbon peapod structure previously seen.[43] The entry of the C_{60} deep into the interior channels of the nanotube is blocked by the encapsulated POM species, resulting in an accumulation of carbon species at the ends of the nanotubes.

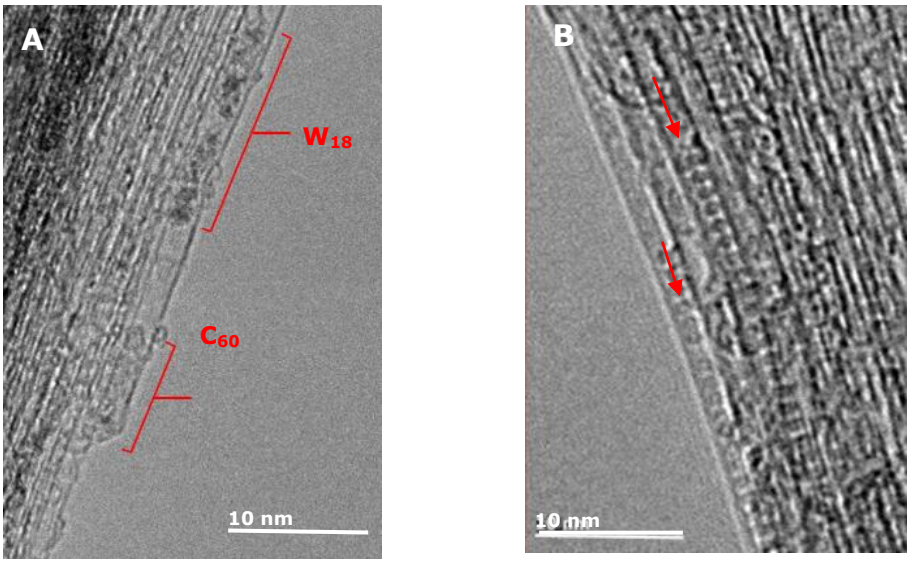

Figure 5. *(A) TEM image of {W_{18}}@SWNT post treatment with fullerene. Focusing on the edge nanotube, where both the encapsulated POM and the carbon matrix blocking the nanotube end can be seen. (B) TEM images of C_{60}@SWNT highlighting two nanotube channels where the 'peapod' structure can be clearly seen.*

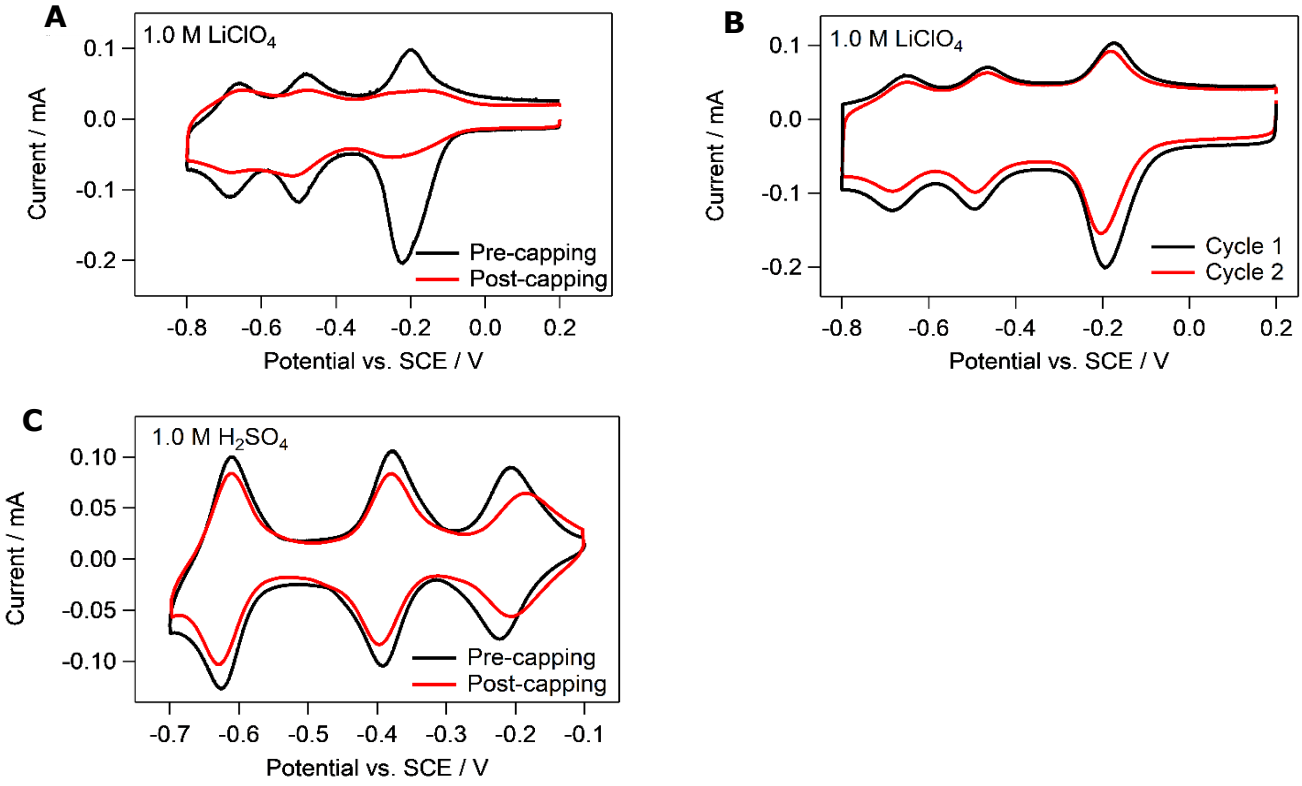

Figure 6. *(A) Cyclic voltammogram of immobilized {W_{18}}@SWNT cycled at 0.1 V s^{-1} in 1.0 mol dm^{-3} $LiClO_4$, pre (black) and post (red) treatment with C_{60}. (B) Cyclic voltammogram of the first (black) and second (red) cycles of immobilized {W_{18}}@SWNT recorded at 0.1 V s^{-1} in 1.0 mol dm^{-3} $LiClO_4$ to indicate the typical current loss observed on subsequent cycles. (C) Cyclic voltammogram of immobilized {W_{18}}@SWNT cycled at 0.1 V s^{-1} in 1.0 mol dm^{-3} H_2SO_4, pre (black) and post (red) treatment with C_{60}.*

Voltammetry in both acidic and non-acidic electrolytes was recorded pre and post capping, to assess the influence this process can have on the different systems. When the capped system was studied in 1 mol dm^{-3} $LiClO_4$ (aq.) a 73.5% decrease in peak current is observed (Figure 6A). For reference, a 22.8% decrease in peak current from one cycle to the next for the uncapped sample of {W_{18}}@SWNT in this electrolyte is typically seen (Figure 6B). On further cycling any electrochemical activity still seen for capped material rapidly fades, which is a synonymous trait for the other non-acidic electrolytes. This indicates that blocking the ends of the nanotube has a profound impact on the electrochemistry displayed by the material

when in environments reliant on the flow of larger cations, confirming that the major pathway leading towards to the POM is no longer accessible to the larger cations.

When considering a system where the mechanism of ion transport does not appear to be sterically hindered, the effect of capping is significantly reduced. Capping experiments conducted in acidic electrolytes exhibit a positive shift in potential of the first redox couple seen as a direct result of the introduction of fullerene to the system. The peak potential positions of the remaining two redox processes remain unchanged (Figure 6C). The minor impact capping appears to have on the system suggests that proton diffusion to the POM is not particularly hindered by the process. This supports the notion that protons can diffuse though the hexagonal lattice of the nanotube sidewall, as a larger impact would be expected from the capping if the only route to access the POM was via the nanotube ends. There is also a possibility that due to their small size protons are still able to permeate through any nanocavities present with the carbon matrix now found at the nanotube ends.

Occasionally decreases in peak currents are observed for post-capped samples, with this affect being more pronounce in the chloride electrolytes, despite this, the electrochemistry of $\{W_{18}\}$@SWNT in acidic environments is always well defined and stable regardless of capping. As there are slight differences observed between the chloride and sulphate electrolytes this indicates that although the cationic species is clearly the prominent factor influencing the electrochemical behaviour of the system, the anion associated to the electrolyte can also be influential.[44,45] Further analysis of this secondary effect has not been carried out within this study.

2.4 Isotopic Influence on {W_{18}}@SWNT Electrochemistry

It can be clearly seen from the cyclic voltammetry data that the effectiveness of charge neutralisation in proton rich environments is considerably more efficient than when this process relies on larger cations. This is supported by the literature which outlines difficulties faced during ion transport through nanoconfined channels for larger cations.[3] Also within the literature, the transport of protons is seen to be matched, albeit to a lesser extent with deuterons.[2,44]

Investigation of the kinetic isotope effect can be pivotal in providing insight into redox mechanisms, in particular those mechanisms involving proton coupled electron transfer.[45-49] Proton coupled electron transfer can be either stepwise or concerted, where the electron transfer and proton transfer occur separately, or simultaneously as part of the same rate-determining step.[50,51] If a kinetic isotope effect is observed, this indicates the proton transfer and electron transfer may occur at different rates.

Cyclic voltammograms of {W_{18}}@SWNT were recorded in 1 mol dm^{-3} DCl and 1 mol dm^{-3} D_2SO_4. As with their protonated counterparts three distinct sets of gaussian surface-confined redox processes were observed (Figure 7A and A5). The positions of these peaks shifted to more positive potentials from HCl to DCl and H_2SO_4 to D_2SO_4 by 28 mV and 26 mV, respectively. As this shift is observed it can be thought of that when in deuterated environments the redox processes occur more readily.

A shift in potential such as this could easily be attributed to differences in pH; redox peaks tend to shift in a positive direction with as pH decreases.[37,52] The pH values for all four acidic electrolytes were recorded on a standard H_2O-calibrates glass electrode pH-meter: 1M HCl (pH 0.33), 1M H_2SO_4 (pH 0.38), 1M DCl (pH*

0.29) and 1M D_2SO_4 (pH* 0.28) (pH* - direct reading of a D_2O solution using H_2O-calibrated pH-meter). Krezel et al. suggested an equation relating the acidities of H2O and D2O solutions measured using glass electrodes:[53]

$$pK^H = 0.929pK^{H*} + 0.42 \quad (4)$$

This equation allows for a direct comparison of pH and pD data, previously this task has had its complications due to the different binding affinities H^+ and D^+ exhibit in solution. Converting the D_2O measured values into H_2O equivalents, takes the measured values of 1M DCl and 1M D_2SO_4 to pH 0.69 and 0.68, respectively. With these relative pH values greater than those observed for their protonated equivalents, a negative potential shift would typically be expected. Suggesting that the observed shift in potentials is not solely as a result of pH differences between the electrolytes but more an intrinsic property of $\{W_{18}\}$@SWNT system.

2.4.1 Kinetic Isotope Effect

Rapid charge transfer kinetics are observed for the system in both protonated and deuterated electrolytes. The kinetic behaviour of these systems was investigated by varying scan rates and using the Laviron method[54,56], this is the perfect system to be studied using the Laviron method due to its surface confined nature. The standard electron transfer rate constant (k_s) and charge transfer coefficient (α) for each redox process can be determined using the relationship between varying peak potentials of both the reduction and oxidation processes and the logarithm of scan rate, as described by equation 4[55]:

$$E_p = E^0 + \left(\frac{RT}{\alpha nF}\right)\left[ln\left(\frac{RTk_s}{\alpha nF}\right) - lnv\right] \quad (5)$$

The standard electron transfer rate constant provides insight into the speed of electron transfer between the POM and the electrode surface at a standard potential and can be related to the rate of ion transport throughout the system. These factors can be determined from the linear portion of the Laviron plot observed at sufficiently high scan rates (example plot found in Figure 7B). For all conditions the asymptotes intersect y=0 at roughly the same point, as alpha falls between the range of 0.3 to 0.7, alpha can be assumed to be 0.5 for all conditions. This assumption results in a relative error of at most 6% on the resulting k_s values.[56]

The rate of electron transfer associated to the three redox couples can be determined and used to compare the apparent rate of diffusion of H^+ and D^+ ions throughout the carbon nanotube network towards the encapsulated POM (Figure 7C, 7D and Table 1). There is a clear decrease in electron transfer rate constant as a result of the deuteration of the supporting electrolyte and solvent. Similar trends are seen between the HCl/DCl and H_2SO_4/D_2SO_4 electrolyte systems, suggesting that for each redox processes the cationic species interacts in a similar manner, albeit slower for the D^+. The average decrease in rate constant is 21.3% and 15.9%, for DCl and D_2SO_4, respectively.

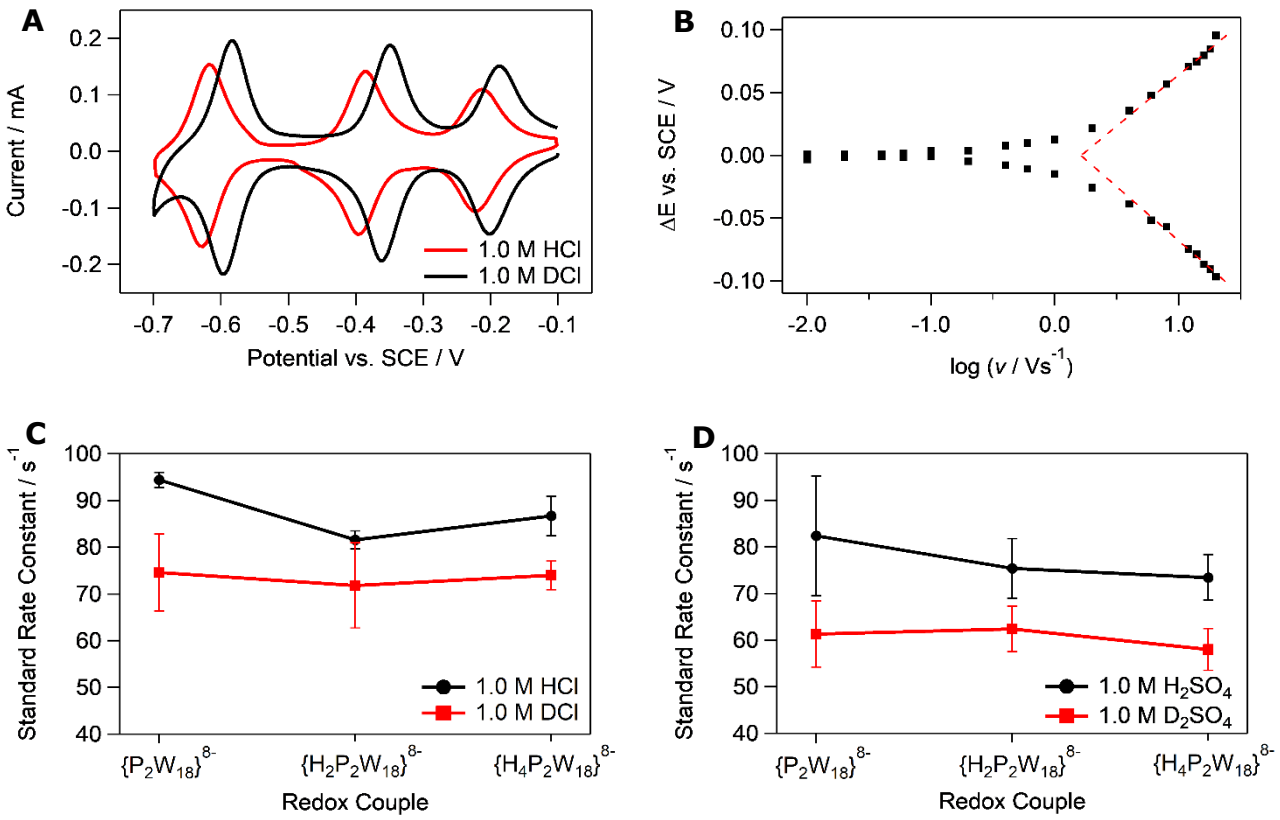

Figure 7. *(A) Cyclic voltammogram of immobilized $\{W_{18}\}$@SWNT recorded at 0.1 V s^{-1} in 1 mol dm^{-3} HCl (red) and 1.0 mol dm^{-3} DCl (black). The differences in currents observed between the H^+ and D^+ voltammograms cannot be solely attributed to the electrolyte as the respective voltammograms are recorded on different electrodes so POM loading is variable and result in different peak currents. (B) Example Laviron plot for the first redox couple in 1.0 mol dm^{-3} H_2SO_4. (C) Rate constants for the three redox couples associated to the electrochemistry of immobilized $\{W_{18}\}$@SWNT in 1.0 mol dm^{-3} HCl (black circles) and 1.0 mol dm^{-3} DCl (red squares). (D) Rate constants for the three redox couples associated to the electrochemistry of immobilized $\{W_{18}\}$@SWNT in 1.0 mol dm^{-3} H_2SO_4 (black circles) and 1.0 mol dm^{-3} D_2SO_4 (red squares).*

Table 1. *Standard rate constants (s^{-1}) for the three redox couples associated to the electrochemistry of immobilized $\{W_{18}\}$@SWNT in 1.0 mol dm^{-3} HCl, 1.0 mol dm^{-3} H_2SO_4, 1.0 mol dm^{-3} DCl and 1.0 mol dm^{-3} D_2SO_4.*

	$\{P_2W_{18}\}^{8-}$	$\{H_2P_2W_{18}\}^{8-}$		$\{H_4P_2W_{18}\}^{8-}$
1 mol dm^{-3} HCl	*82.4*	*75.4*	*73.4*	
1 mol dm^{-3} H_2SO_4	*94.4*	*81.6*		*86.7*
1 mol dm^{-3} DCl	*61.3*	*62.4*		*58.0*
1 mol dm^{-3} D_2SO_4	*74.6*	*71.8*		*74.0*

Using the ratio of the rates calculated using the Laviron method for both the protonated and deuterated systems, the kinetic isotope effect (KIE) for these systems can be estimated. The average values for the KIE were found to be 1.27 and 1.19 for the HCl and H_2SO_4 systems respectively, these ratios are in roughly in agreement with the mobilities expected for H^+ and D^+ in the measured environments. The ratio of mobilities of H^+ in H_2O and D^+ in D_2O (at 25°C) is 1.41[57], this is consistent with the diffusion rate expected for classical particles and is rationalized to be approximately inversely proportional to $\sqrt{m}$.[44] A KIE around this value, could suggest that the rate limiting step can be attributed to the behaviour of the ions in the bulk solution.[46,48]

It can be difficult to compare values found for the electron transfer kinetics of other systems as the POM structural type and electrode substrate can influence the kinetics massively.[58] Literature shows rate constant values for POM-based systems can vary by a factor of 100.[56,59-63] High electron transfer rate constant values ($\leq 500\ s^{-1}$) have been observed for a selection of POM systems, some of these values are considerably higher than the rate constants reported here.[61] When the system in question was subjected to the addition of a strong acid the POM reduction was seen to be thermodynamically facilitated (as seen in our system by the shifting of the electrochemical waves to higher potentials when in the presence of acidic electrolytes). However, this gain was found to be at the expense of the kinetics of the electron transfer whereby the rate constant was seen to decrease more than ten-fold ($12\ s^{-1}$).[61] This indicates that our $\{W_{18}\}$@SWNT film does exhibit relatively high rate constant values when measured in an acidic environment; the enhanced kinetics could be partially

attributed to the presence of the conductive carbon nanotube substrate.

Although both systems exhibited rapid charge transfer kinetics, there is potential to exploit the system further to access even larger rate constants. It is naïve to assume that the existing $\{W_{18}\}$@SWNT film studied here is a perfect monolayer immobilized onto the electrode surface. Heterogeneities and multilayer characteristics may be present within the system, potentially due to a degree of nanotube stacking within the film. When studying a multilayer surface-confined system it is important to consider diffusion-limitation within the system which can be attributed to the movement of electrons and counter ions between the redox centres found within the film.[58] This effect is seen to a lesser extent within monolayer systems. By isolating a perfect monolayer of $\{W_{18}\}$@SWNT there is the opportunity to reduce the impact of this diffusion process and hence result in faster overall charge transfer rate constants.[60]

Investigations into the permeation of hydrogen isotopes through one-atom-thick crystals such as graphene, a comparable material to the CNT sidewalls, suggest a substantial isotopic effect.[2] With the rate of hydron transport varying by approximately a factor of 10, due to the differences in activation barriers posed by the two-dimensional crystals studied for the two isotope species. We do not see a relationship such as this, indicating that our system is not limited by the rate of permeation of ions through the film. Hence, the proton coupled electron transfer exhibited by this system proceeds in a stepwise fashion. Although the transport of D^+ may be restricted in comparison to H^+ as suggested in the literature, the process is still suitability fast for application within a practical electrochemical system.

3. Conclusion

A fundamentally simple system of {W_{18}}@SWNT has been utilized to provide insight into the transport of cationic species within carbon nanotubes. The polyoxometalate, W_{18}, acts as probe to measure the electrochemical response of the system, however any redox active species could be used assuming that they too can be encapsulated. Excellent redox properties are measured in acidic environments, for both H^+ and D^+ containing environments, however, limitations are seen for environments relying on the transport of larger cations (Li^+, Na^+, K^+, NH_4^+) throughout the CNT matrix.

Capping the ends of the {W_{18}}@SWNT with C_{60} provided evidence to support proposed mechanisms of cation transport throughout the nanotube system. Significant decrease in current was observed when measuring the electrochemistry of the encapsulated POM within the capped system when studied in non-acidic electrolytes. Suggesting larger cations flow through the ends of the nanotubes and are unable to diffuse through the nanotube walls. The impact of capping is considerably less significant when studied in acidic electrolytes suggesting smaller cations such as H^+ and D^+ can diffuse through both the ends and the sidewalls of the nanotubes.

The permeation of H^+ and D^+ through the CNT is not rate limiting and occurs sufficiently fast for efficient reversible electrochemistry to occur. Consequently, kinetic isotope effects do not limit the use of deuterated acidic electrolytes for practical application in electrochemical systems that rely on the permeation of ions through two-dimensional crystals.

4. Future Work

The simplicity of this electrochemical system lends itself to a host of further applications. If the method of spontaneous encapsulation can be utilised for a variety of redox active species, and similar electrochemical measurements can be carried out. Then the practical applications of X@SWNT as fundamental systems whereby ion transport can be assessed, can be confirmed. The successful encapsulation of other POM species has already been reported.[1] The electrochemical responses seen of these materials in various supporting electrolytes indicate the versatility of ion transport study using nanoconfined redox active species.

Due to the redox capabilities and stability of W_{18}@SWNT within H^+ and D^+ rich environments, it is key to test the material in a more practical sense to assess their potential as electrode materials for energy storage applications.

5. Experimental

$K_6[P_2W_{18}O_{62}](H_2O)_{14}$ was synthesised using literature methods[64], by another chemist.

To synthesis the POM@SWNT consisted of heating SWNTs (20 mg) at 600 °C for 30 minutes. The resulting black solid (10 mg) was sonicated briefly in a POM solution (100 mg $K_6[P_2W_{18}O_{62}](H_2O)_{14}$ in 3 mL water). The resultant suspension was then stirred at room temperature for two days and filtered through a PTFE membrane (0.2 μm) to give a black solid.

The electrochemistry measurements were recorded using a CHI760C potentiostat (CH Instruments). All measurements were carried out in a three-electrode electrochemical cell which comprises of a glassy carbon (GC) disc (3 mm diameter) working electrode, a GC rod counter electrode, and a saturated calomel reference electrode. Suspensions of 1 wt. % POM@SWNT and 3 wt. % polytetrafluoroethylene binder were prepared via sonication for 20 minutes, resulting in a black ink. 8 μL of the aqueous POM@SWNT ink was deposited onto the GC electrode surface and allowed to dry, resulting in a POM@SWNT film adsorbed onto the surface. To prepare the electrode before the POM@SWNT is added, the GC electrode was polished on felt polishing pads using aqueous alumina suspensions of increasing particulate size; 0.05 μm, 0.3 μm, 1.0 μm. The electrodes were placed in 5 mL of electrolyte solution, which was purged of air and the system was kept in an Ar atmosphere during the measurements.

The method of capping the electrode is as follows: 10 μL of 2.77 mM fullerene in toluene suspension was drop-casted onto a dried glassy carbon POM@SWNT coated electrode, and allowed to dry, once dried 10 μL of toluene was added to

aid the capping process.

Samples analysed via transmission electron microscopy (TEM) were prepared by sonicating the POM@CNT composites in propan-2-ol, which was then drop cast onto lacey carbon-coated copped TEM grids. The images were generated using a JEOL 2100+ TEM microscope, operated at 80 kV.

6. References

(1) Hu, S.; Lozada-Hidalgo, M.; Wang, F. C.; Mishchenko, A.; Schedin, F.; Nair, R. R.; Hill, E. W.; Boukhvalov, D. W.; Katsnelson, M. I.; Dryfe, R. A. W.; Grigorieva, I. V.; Wu, H. A.; Geim, A. K. Proton Transport through One-Atom-Thick Crystals. *Nature* **2014**, *516* (7530), 227–230. https://doi.org/10.1038/nature14015.

(2) Lozada-Hidalgo, M.; Hu, S.; Marshall, O.; Mishchenko, A.; Grigorenko, A. N.; Dryfe, R. A. W.; Radha, B.; Grigorieva, I. V.; Geim, A. K. Sieving Hydrogen Isotopes through Two-Dimensional Crystals. *Science (80-.).* **2016**, *351* (6268), 68–70. https://doi.org/10.1126/science.aac9726.

(3) Gopinadhan, K.; Hu, S.; Esfandiar, A.; Lozada-Hidalgo, M.; Wang, F. C.; Yang, Q.; Tyurnina, A. V.; Keerthi, A.; Radha, B.; Geim, A. K. Complete Steric Exclusion of Ions and Proton Transport through Confined Monolayer Water. *Science (80-.).* **2019**, *363* (6423), 145–148. https://doi.org/10.1126/science.aau6771.

(4) Mogg, L.; Zhang, S.; Hao, G.-P.; Gopinadhan, K.; Barry, D.; Liu, B. L.; Cheng, H. M.; Geim, A. K.; Lozada-Hidalgo, M. *Perfect Proton Selectivity in Ion Transport through Two-Dimensional Crystals*.

(5) Salanne, M.; Rotenberg, B.; Naoi, K.; Kaneko, K.; Taberna, P. L.; Grey, C. P.; Dunn, B.; Simon, P. Efficient Storage Mechanisms for Building Better Supercapacitors. *Nature Energy*. Nature Publishing Group May 9, 2016, pp 1–10. https://doi.org/10.1038/nenergy.2016.70.

(6) Berry, V. Impermeability of Graphene and Its Applications. *Carbon*. Pergamon October 1, 2013, pp 1–10. https://doi.org/10.1016/j.carbon.2013.05.052.

(7) Norby, T. Solid-State Protonic Conductors: Principles, Properties, Progress and Prospects. *Solid State Ionics* **1999**, *125* (1), 1–11. https://doi.org/10.1016/S0167-2738(99)00152-6.

(8) Yuan, W.; Chen, J.; Shi, G. Nanoporous Graphene Materials. *Materials Today*. Elsevier March 1, 2014, pp 77–85. https://doi.org/10.1016/j.mattod.2014.01.021.

(9) Garaj, S.; Hubbard, W.; Reina, A.; Kong, J.; Branton, D.; Golovchenko, J. A. Graphene as a Subnanometre Trans-Electrode Membrane. *Nature* **2010**, *467* (7312), 190–193. https://doi.org/10.1038/nature09379.

(10) O'Hern, S. C.; Boutilier, M. S. H.; Idrobo, J. C.; Song, Y.; Kong, J.; Laoui, T.; Atieh, M.; Karnik, R. Selective Ionic Transport through Tunable Subnanometer Pores in Single-Layer Graphene Membranes. *Nano Lett.* **2014**, *14* (3), 1234–1241. https://doi.org/10.1021/nl404118f.

(11) Sint, K.; Wang, B.; Král, P. Selective Ion Passage through Functionalized Graphene Nanopores. *J. AM. CHEM. SOC* **2008**, *130*, 47. https://doi.org/10.1021/ja804409f.

(12) Yazda, K.; Tahir, S.; Michel, T.; Loubet, B.; Manghi, M.; Bentin, J.; Picaud, F.; Palmeri, J.; Henn, F.; Jourdain, V. Voltage-Activated Transport of Ions through Single-Walled Carbon Nanotubes †. *Nanoscale* **2017**, *9*. https://doi.org/10.1039/c7nr02976d.

(13) Pham, X. H.; Bui, M. P. N.; Li, C. A.; Han, K. N.; Kim, J. H.; Won, H.; Seong, G. H. Electrochemical Characterization of a Single-Walled Carbon Nanotube Electrode for Detection of Glucose. *Anal. Chim. Acta* **2010**, *671* (1–2), 36–40. https://doi.org/10.1016/j.aca.2010.05.010.

(14) Yu, M.; Funke, H. H.; Falconer, J. L.; Noble, R. D. Gated Ion Transport through Dense Carbon Nanotube Membranes. https://doi.org/10.1021/ja9091769.

(15) Rollings, R. C.; Kuan, A. T.; Golovchenko, J. A. ARTICLE Ion Selectivity of Graphene Nanopores. *Nat. Commun.* **2016**. https://doi.org/10.1038/ncomms11408.

(16) Sinclair, R. C.; Suter, J. L.; Coveney, P. V. Micromechanical Exfoliation of Graphene on the Atomistic Scale. *Phys. Chem. Chem. Phys.* **2019**, *21* (10), 5716–5722. https://doi.org/10.1039/c8cp07796g.

(17) Jordan, J. W.; Lowe, G. A.; McSweeney, R. L.; Stoppiello, C. T.; Lodge, R. W.; Skowron, S. T.; Biskupek, J.; Rance, G. A.; Kaiser, U.; Walsh, D. A.; Newton, G. N.; Khlobystov, A. N. Host–Guest Hybrid Redox Materials Self-Assembled from Polyoxometalates and Single-Walled Carbon Nanotubes. *Adv. Mater.* **2019**, *31* (41), 2–6. https://doi.org/10.1002/adma.201904182

(18) Ammam, M. Polyoxometalates: formation, structutes, principal properties, main deposition and applications in sensing. *J. Mater. Chem. A*. **2013**, *1*, 6291-6312. https://doi.org/10.1039/C3TA01663C

(19) Long, D.; Burkholder, E.; Cronin, L. Polyoxometalate Clusters, Nanostructure and Materials: From Self Assembly to Designer Materials and Devices. *Chem. Soc. Rev.* **2007**, *36*, 105-121. https://doi.org/10.1039/B502666K

(20) Cameron, J. M.; Wales, D. J.; Newton, G. N. Shining a Light on the Photo-Sensitisation of Organic-Inorganic Hybrid Polyoxometalates. *Dalton Trans.* **2018**, *47*, 5120-5136. https://doi.org/10.1039/C8DT00400E

(21) Mortiboy, B. (2019). *Invesitgation into the Electrochemnical Properties of Polyoxometalates Encapsulate in Single-Walled Nanotubes* [Unpublished Master's thesis]. University of Nottingham.

(22) Gumerova, N. I.; Rompel, A. Synthesis, Structures and Applications of Electron-Rich Polyoxometalates. *Nat. Rev. Chem*. **2018**, *2* (0112).

https://doi.org/10.1038/s41570-018-0112

(23) McSweeney, R. L.; Chamberlain, T. W.; Baldoni, M.; Lebedeva, M. A.; Davies, E. S.; Besley, E.; Khlobystov, A. N. Direct Measurement of Electron Transfer in Nanoscale Host-Guest Systems: Metallocenes in Carbon Nanotubes. *Chem. Eur. J.* **2016**, *22* (38), 13540-13549. https://doi.org/10.1002/chem.201602116

(24) Kawasaki, N.; Wang, H.; Nakanishi, R.; Hamanaka, S.; Kitaura, R.; Shinohara, H.; Yokoyama, T.; Yoshikawa, H.; Awaga, K. Nanohybridization of Polyoxometalate Clusters and Single-Wall Carbon Nanotubes: Applications in Molecular Cluster Batteries. *Angew. Chemie Int. Ed.* **2011**, *50* (15), 3471–3474. https://doi.org/10.1002/anie.201007264

(25) Wang, Y.; Weinstock, I. A. Cation Mediated Self-Assembly of Inorganic Cluster Anion Building Blocks. **2010**. https://doi.org/10.1039/c0dt00166j.

(26) Britz Ab, D. A.; Khlobystov, A. N. Noncovalent Interactions of Molecules with Single Walled Carbon Nanotubes. **2002**. https://doi.org/10.1039/b507451g.

(27) Pope, M. T.; Varga, G. M. Heteropoly blues. I. Reduction stoichiometries and reduction potentials of some 12-tungstates. *Inorg. Chem.* **1966**, *5*, 1249-1254. https://doi.org/10.1021/ic50041a038

(28) Pope, M. T.; Papaconstantinou, E. Heteropoly blues. II. Reduction of 2:18-tungstates. *Inorg. Chem.* **1967**, *6* (6), 1147-1152. https://doi.org/10.1021/ic50052a018

(29) Elgrishi, N. N.; Rountree, K. J.; Mccarthy, B. D.; Rountree, E. S.; Eisenhart, T. T.; Dempsey, J. L. A Practical Beginner's Guide to Cyclic Voltammetry. *J. Chem. Educ.* **2017**, *95* (2), 197-206. https://doi.org/10.1021/acs.jchemed.7b00361.

(30) Weaver, M. J.; Liu, H. Y.; Kim, Y.; The Role of the Supporting Electrolyte Cation in the Kinetics of Outer-Sphere Electrochemical Redox Processes Involving Metal Complexes. *Can. J. Chem.* **1981**, *59,* 1944-1953.

(31) Choi, W.; Ulissi, Z. W.; Shimizu, S. F. E.; Bellisario, D. O.; Ellison, M. D.; Strano, M. S. Diameter-Dependent Ion Transport through the Interior of Isolated Single-Walled Carbon Nanotubes. *Nat. Commun.* **2013**, *4* (2397). https://doi.org/10.1038/ncomms3397.

(32) Tunuguntla, R. H.; Allen, F. I.; Kim, K.; Belliveau, A.; Noy, A. Ultrafast Proton Transport in Sub-1-Nm Diameter Carbon Nanotube Porins. *Nat. Nanotechnol.* **2016**, *11* (7), 639-644. https://doi.org/10.1038/NNANO.2016.43.

(33) Huang, L.; Wu, B.; Yu, G.; Liu, Y. Graphene: Learning from Carbon Nanotubes. *J. Mater. Chem*. **2011**, *21*, 901–1272. https://doi.org/10.1039/c0jm02225j.

(34) Bukola, S.; Liang, Y.; Korzeniewski, C.; Harris, J.; Creager, S. Selective Proton/Deuteron Transport through Nafion|Graphene|Nafion Sandwich Structures at High Current Density. *J. Am. Chem. Soc.* **2018**, *140* (5), 1743–1752. https://doi.org/10.1021/jacs.7b10853.

(35) Achtyl, J. L.; Unocic, R. R.; Xu, L.; Cai, Y.; Raju, M.; Zhang, W.; Sacci, R. L.; Vlassiouk, I. V.; Fulvio, P. F.; Ganesh, P.; Wesolowski, D. J.; Dai, S.; Van Duin, A. C. T.; Neurock, M.; Geiger, F. M. Aqueous Proton Transfer across Single-Layer Graphene. *Nat. Commun.* **2015**, *6*, 1–7. https://doi.org/10.1038/ncomms7539.

(36) Mogg, L.; Hao, G. P.; Zhang, S.; Bacaksiz, C.; Zou, Y. C.; Haigh, S. J.; Peeters, F. M.; Geim, A. K.; Lozada-Hidalgo, M. Atomically Thin Micas as Proton-Conducting Membranes. *Nat. Nanotechnol.* **2019**, *14* (10), 962-966. https://doi.org/10.1038/s41565-019-0536-5.

(37) Sadakane, M.; Steckhan, E. Electrochemical Properties of Polyoxometalates as Electrocatalysts. *Chem. Rev.* **1998**, *98* (1), 219-238. doi: 10.1021/cr960403a.

(38) Keita, B.; Nadjo, L. New Aspects of the Electrochemistry of Heteropolyacids. Part IV. Acidity Dependent Cyclic Voltammetric Behaviour of Phosphotungstic and Silicotungstic Heteropolyanions in Water and N,N-Dimethylformamide. *J. Electroanal. Chem.* **1987**, *227* (1–2), 77–98. https://doi.org/10.1016/0022-0728(87)80067-0.

(39) Bonin, J.; Costentin, C.; Robert, M.; Routier, M.; Saveánt, J.-M. Proton-Coupled Electron Transfers: PH-Dependent Driving Forces? Fundamentals and Artifacts. *J. Am. Chem. Soc.* **2013**, *135* (38), 14359-14366. https://doi.org/10.1021/ja406712c.

(40) Kubota, S.; Ozaki, S.; Onishi, J.; Kano, K.; Shirai, O. Selectivity on Ion Transport across Bilayer Lipid Membranes in the Presence of Gramicidin A. *Anal. Sci.* **2009**, *25* (2), 189–194. https://doi.org/10.2116/analsci.25.189.

(41) Liu, J.; Shi, G.; Guo, P.; Yang, J.; Fang, H. Blockage of Water Flow in Carbon Nanotubes by Ions Due to Interactions between Cations and Aromatic Rings. *Phys. Rev. Lett* **2015**, *115* (16), 164502. https://doi.org/10.1103/PhysRevLett.115.164502.

(42) Bird, M. A.; Goodwin, S. E.; Walsh, D. A. Best Practice for Evaluating Electrocatalysts for Hydrogen Economy. *ACS Appl. Mater. Interfaces* **2020**,*12* (18), 20500-20506.

(43) Smith, B. W.; Monthioux, M.; Luzzi, D. E. Encapsulated C60 in Carbon Nanotubes [7]. *Nature*. Macmillan Magazines Ltd November 26, 1998, pp 323–324. https://doi.org/10.1038/24521.

(44) Chen, C.; Huang, C.; Waluyo, I.; Weiss, T.; Pettersson, L. G. M.; Nilsson, A. Long-Range Ion-Water and Ion-Ion Interactions in Aqueous Solutions. *Phys. Chem. Chem. Phys.* **2015**, *17* (13), 8427–8430.

(45) Banerjee, P.; Bagchi, B. Ions' Motion in Water. *J. Chem. Phys.* **2019**, *150*, 190901. https://doi.org/10.1063/1.5090765.

(46) Hu, S.; Gopinadhan, K.; Rakowski, A.; Neek-Amal, M.; Heine, T.; Grigorieva, I. V.; Haigh, S. J.; Peeters, F. M.; Geim, A. K.; Lozada-Hidalgo, M. Transport of Hydrogen Isotopes through Interlayer Spacing in van Der Waals Crystals. *Nat. Nanotechnol.* **2018**, *13* (6), 468–472. https://doi.org/10.1038/s41565-018-0088-0.

(47) Le Coutre, J.; Gerwert, K. Kinetic Isotope Effects Reveal an Ice-like and a Liquid-Phase-Type Intramolecular Proton Transfer in Bacteriorhodopsin. *FEBS Lett.* **1996**, *398* (2–3), 333–336. https://doi.org/10.1016/S0014-5793(96)01254-9.

(48) DeCoursey, T. E.; Cherny, V. V; or, O. D. *Deuterium Isotope Effects on Permeation and Gating of Proton Channels in Rat Alveolar Epithelium*; 1997; Vol. 109.

(49) Karpefors, M.; Ädelroth, P.; Brzezinski, P. The Onset of the Deuterium Isotope Effect in Cytochrome c Oxidase. *Biochemistry.* **2000**, *39* (17), 5045–5050. https://doi.org/10.1021/bi9925221.

(50) Springer, A.; Hagen, V.; Cherepanov, D. A.; Antonenko, Y. N.; Pohl, P. Protons Migrate along Interfacial Water without Significant Contributions from Jumps between Ionizable Groups on the Membrane Surface. *PNAS.* **2011**, *108*. https://doi.org/10.1073/pnas.1107476108/-/DCSupplemental.

(51) Hammes-Schiffer, S. Kinetic Isotope Effects for Proton-Coupled Electron Transfer Reactions. *ChemInform.* **2006**, *37* (31), no-no. https://doi.org/10.1002/chin.200631263.

(52) Sobczak, A.; Rebiś, T.; Milczarek, G. Electrocatalysis of NADH Oxidation Using Electrochemically Activated Fluphenazine on Carbon Nanotube Electrode. *Bioelectrochemistry.* **2015**, *106*, 308–315.

(53) Krężel, A.; Bal, W. A Formula for Correlating PKa Values Determined in D_2O and H_2O. *J. Inorg. Biochem.* **2004**, *98* (1), 161–166.

(54) Eckermann, A. L.; Feld, D. J.; Shaw, J. A.; Meade, T. J. Electrochemistry of Redox-Active Self-Assembled Monolayers. *Coord. Chem. Rev.* **2010**, *254* (15-16), 1769-1802. https://doi.org/10.1016/j.ccr.2009.12.023.

(55) Sjödin, M.; Hjelm, J.; Rutherford, A. W.; Forster, R. Proton-Coupled Electron Transfer from an Interfacial Phenol Monolayer. *J. Electroanal. Chem.* **2020**, *859*, 113856. https://doi.org/10.1016/j.jelechem.2020.113856.

(56) Laviron, E. General Expression of the Linear Potential Sweep Voltammogram in the Case of Diffusionless Electrochemical Systems. *J. Electroanal. Chem.* **1979**, *101* (1), 19–28. https://doi.org/10.1016/S0022-0728(79)80075-3.

(57) Fotouhi, L.; Hashkavayi, A. B.; Heravi, M. M. Electrochemical Behaviour and Voltammetric Determination of Sulphadiazine Using a Multi-Walled Carbon Nanotube Composite Film-Glassy Carbon Electrode. *J. Exp. Nanoscience.* **2012**, *8* (7-8), 947-956. https://doi.org/10.1080/17458080.2011.624554.

(58) Conway, B. E.; Bockris, M.; Linton, H. Proton Conductance and the Existence of the $H_3O\cdot$ Ion. *J. Chem. Phys* **1956**, *24*, 834. https://doi.org/10.1063/1.1742619.

(59) Rinfray, C.; Izzet, G.; Pinson, J.; Gam Derouich , S.; Ganem, J.-J.; Combellas, C.; Kanoufi, F.; Proust, A. Electrografting of Diazonium-Functionalized Polyoxometalates: Synthesis, Immobilisation and Electron-Transfer Characterisation from Glassy Carbon. *Chem. - A Eur. J.* **2013**, *19* (41), 13838–13846. https://doi.org/10.1002/chem.201302304.

(60) Gam Derouich, S.; Rinfray, C.; Izzet, G.; Pinson, J.; Gallet, J. J.; Kanoufi, F.; Proust, A.; Combellas, C. Control of the Grafting of Hybrid Polyoxometalates on Metal and Carbon Surfaces: Toward Submonolayers. *Langmuir* **2014**, *30* (8), 2287–2296. https://doi.org/10.1021/la500067e.

(61) Rinfray, C.; Brasiliense, V.; Izzet, G.; Volatron, F.; Alves, S.; Combellas, C.; Kanoufi, F.; Proust, A. Electron Transfer to a Phosphomolybdate Monolayer on Glassy Carbon: Ambivalent Effect of Protonation. *Inorg. Chem.* **2016**, *55* (14), 6929-6937. https://doi.org/10.1021/acs.inorgchem.6b00485

(62) Salimi, A.; Korani, A.; Hallaj, R.: Khoshnavazi, R.; Hadadzadeh. Immobilization of $[Cu(bpy)_2]Br_2$ complex onto a glassy carbon electrode modified with α-$SiMo_{12}O_{40}^{4-}$ and single walled carbon nanotubes: Application to nanomolar detection of hydrogen peroxide and bromate. *Anal. Chim. Acta.* **2009**, *635* (1), 63-70. https://doi.org/10.1016/j.aca.2009.01.007

(63) Volatron, F.; Noël, J.;Rinfray, C.; Decorse, P.; Combellas, C.; Kanoufi, F.; Proust, A. Electron Transfer Properties of a Monolayer of Hybrid Polyoxometalates on Silicon. *J. Mater. Chem. C.* **2015**, *3*, 6266-6275. https://doi.org/10.1039/C5TC00074B

(64) Graham, C. R.; Finke, R. G. The classic Wells-Dawson polyoxometalate, K_6[alpha-$P_2W_{18}O_{62}$].14H_2O. Answering an 88 year-old question: what is its preferred, optimum synthesis?. *Inorg. Chem*. **2008**, *47*(9), 3679-3686.

7. Appendix

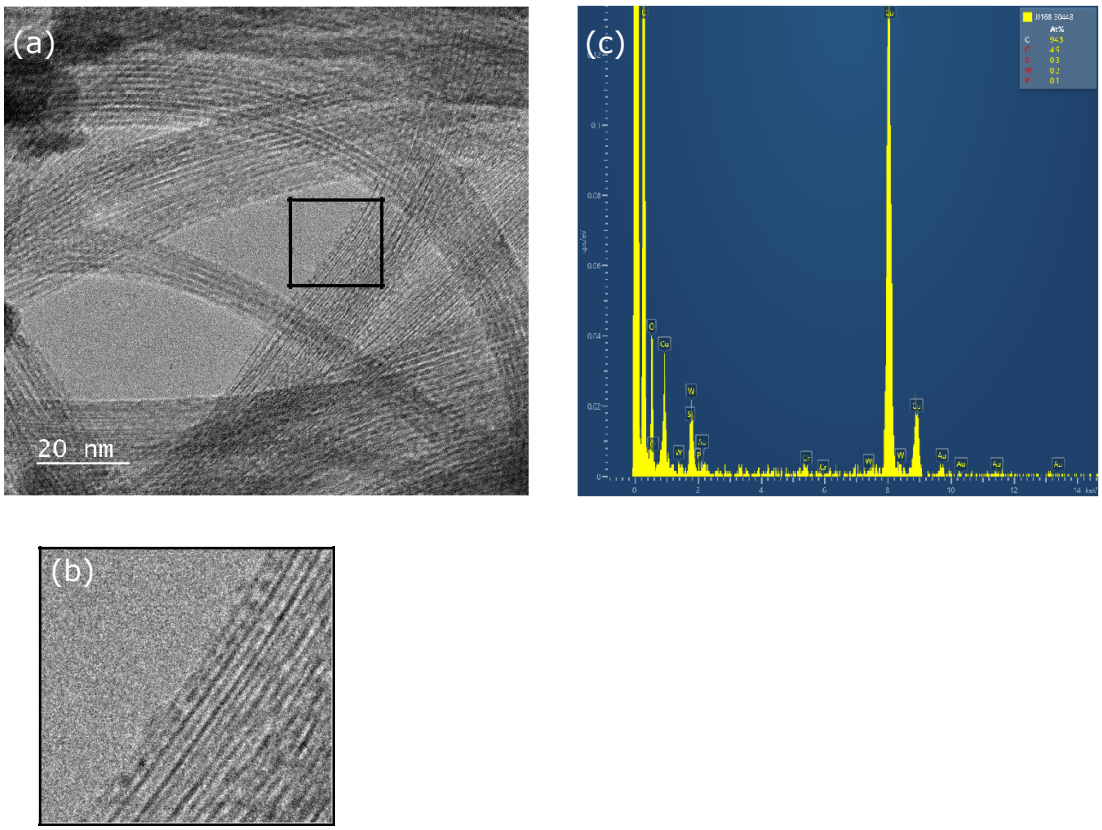

Figure A1. *TEM images of {W_{18}}@SWNT - The TEM images show the typical 'peapod' arrangement of POMs within a SWNT. By approximately measuring these molecules, their average size is seen to be 1.2 nm, which is in good agreement of the expected size of a Wells-Dawson POM (1.4 nm x 1 nm). a) complete image, b) 20 nm x 20 nm image highlighted by the black box in image a, providing a closer view of the POM 'peapod' arrangement. The images were collected at an accelerating voltage of 80 kV. c) EDX spectra of {W_{18}}@SWNT confirming the presence of all elements found within the POM (phosphorous, tungsten and oxygen) in the {W_{18}}@SWNT sample.*

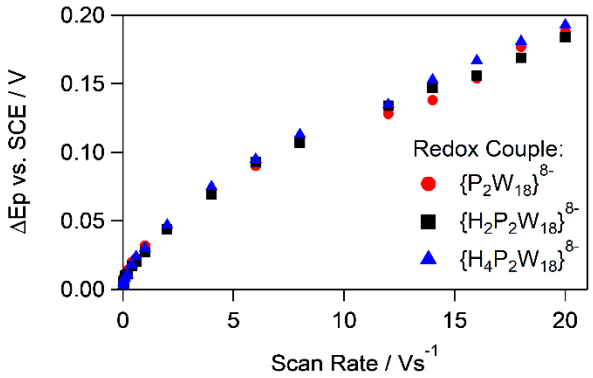

Figure A2. *Plot of peak-to-peak separation as a function of scan rate for the three redox couples seen in figure 3E.*

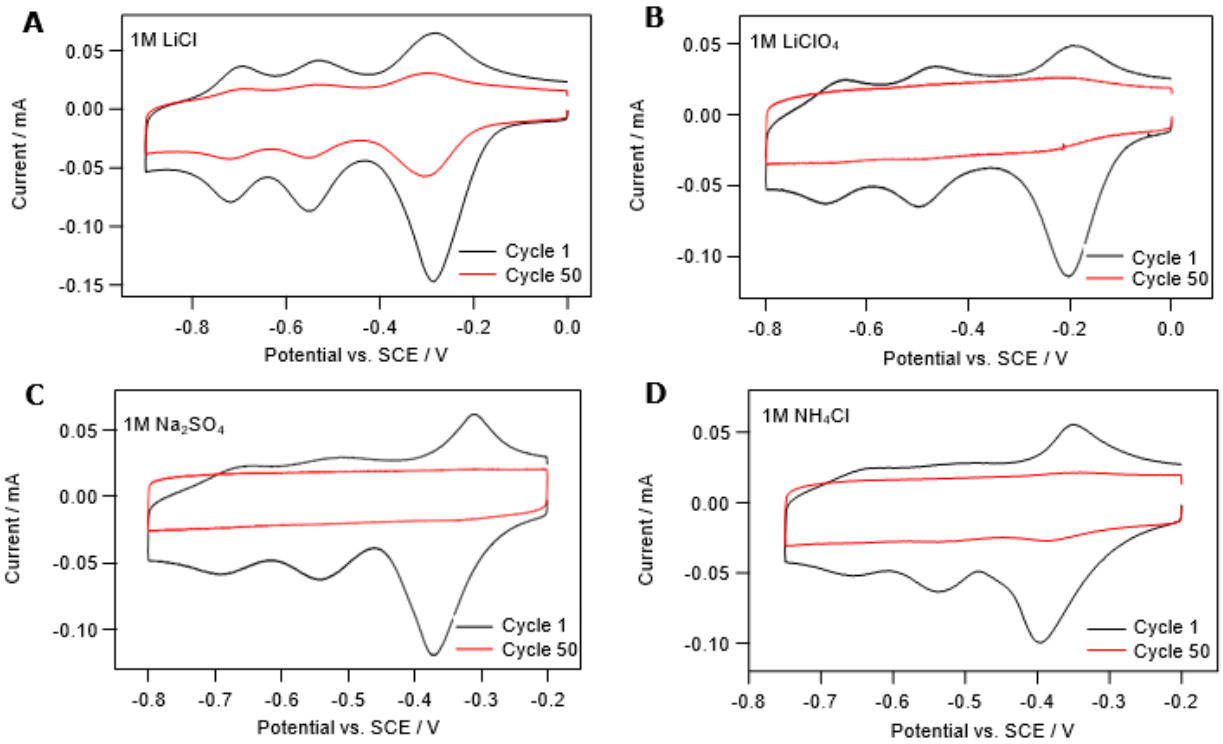

Figure A3. *First and 50th cyclic voltammograms of {W_{18}}@SWNT deposited onto a glassy carbon electrode and cycled at 0.1 mV s^{-1} in (A) 1M LiCl, (B) 1M $LiClO_4$, (C)1M Na_2SO_4 and (D) 1M NH_4Cl.*

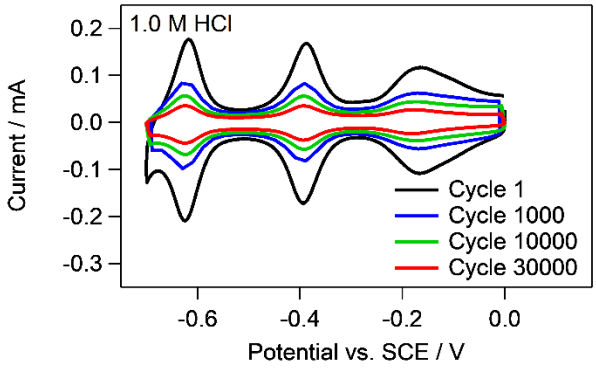

Figure A4. *1st to 30,000th cyclic voltammograms of {W_{18}}@SWNT deposited onto a glassy carbon electrode and cycled at 0.1 V s^{-1} in 1.0 mol dm^{-3} HCl.*

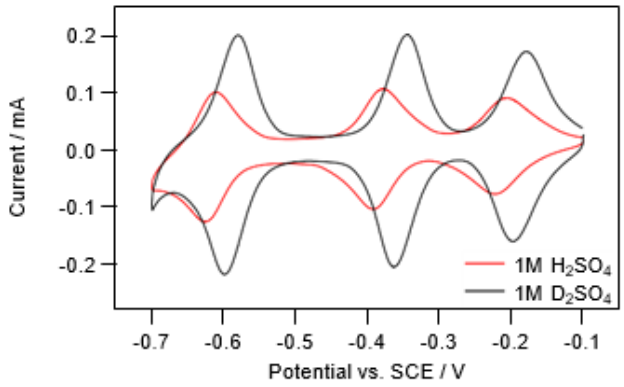

Figure A5. *Cyclic voltammogram of immobilized {W_{18}}@SWNT recorded at 0.1 V s^{-1} in 1 mol dm^{-3} H_2SO_4 (red) and 1.0 mol dm^{-3} D_2SO_4 (black). The differences in currents observed between the H^+ and D^+ voltammograms cannot be solely attributed to the electrolyte as the respective voltammograms are recorded on different electrodes so POM loading is variable and result in different peak currents.*

8. Acknowledgements

I would like to thank my supervisors Dr. Darren Walsh and Dr. Graham Newton for their continued support, both personally and scientifically. Additionally, I wish to thank Prof. Andrei Khlobystov for his sustained enthusiasm for this research. I would also like to thank Jack Jordan, initially for sharing your findings and materials with me, which allowed this research to take be completed. But also, for acquiring the TEM images presented within this paper and more importantly for all of the support you have given me from the start of this project until now. Finally, I wish to thank the LDMI Doctoral Training Programme for funding.